Experimental study of the low-lying negative-parity states in ^{11}Be using the ^{12}B(d, ^{3}He)^{11}Be reaction

J. Chen,[1,*] K. Auranen,[1,†] M. L. Avila,[1] B. B. Back,[1] M. A. Caprio,[2] C. R. Hoffman,[1] D. Gorelov,[3,1] B. P. Kay,[1] S. A. Kuvin,[4] Q. Liu,[5] J. L. Lou,[5] A. O. Macchiavelli,[6] D. G. McNeel,[4] T. L. Tang,[1] D. Santiago-Gonzalez,[1] R. Talwar,[1] J. Wu,[1] G. Wilson,[7,1] R. B. Wiringa,[1] Y. L. Ye,[5] C. X. Yuan,[8] and H. L. Zang[5]

[1]*Physics Division, Argonne National Laboratory, Argonne, Illinois 60439, USA*
[2]*Department of Physics, University of Notre Dame, Notre Dame, Indiana 46556, USA*
[3]*Department of Physics and Astronomy, University of Manitoba, Allen Building, Winnipeg MB R3T 2N2, Canada*
[4]*Department of Physics, University of Connecticut, Storrs, Connecticut 06269, USA*
[5]*School of Physics, State Key Laboratory of Nuclear Physics and Technology, Peking University, Beijing 100871, China*
[6]*Nuclear Science Division, Lawrence Berkeley National Laboratory, Berkeley, California 94720, USA*
[7]*Department of Physics and Astronomy, Louisiana State University, Baton Rouge, Louisiana 70803, USA*
[8]*Sino-French Institute of Nuclear Engineering and Technology, Sun Yat-Sen University, Zhuhai 519082, China*

(Received 22 September 2019; published 20 December 2019)

Low-lying negative-parity states in ^{11}Be having dominant p-wave neutron configurations were studied using the ^{12}B(d, ^{3}He)^{11}Be proton-removal reaction in inverse kinematics. The $1/2^-_1$ state at 0.32 MeV, the $3/2^-_1$ state at 2.56 MeV, and one or both of the states including the $5/2^-_1$ level at 3.89 MeV and the $3/2^-_2$ level at 3.96 MeV were populated in the present reaction. Spectroscopic factors were determined from the differential cross sections using a distorted wave Born approximation method. The p-wave proton removal strengths were well described by the shell model calculations while the Nilsson model calculation underestimates the spectroscopic factors for the higher excited states. Results from both variational Monte Carlo and no-core shell-model calculations were also compared with the experimental observations.

DOI: 10.1103/PhysRevC.100.064314

I. INTRODUCTION

In light nuclei, the structure of the Be isotopes provides a great testing ground for numerous complementary nuclear models. The small number of valence nucleons allows for in-depth tests of the approximations made in single-particle calculations based on effective interactions in the shell model as well as more fundamentally based *ab initio* calculations. In addition, the observation of structures with "deformation" properties in these isotopes opens an avenue for testing the validity of the Nilsson model or cluster model descriptions.

The duality of the collective and single-particle descriptions of the structure of the atomic nucleus has been probed by recent experimental work on ^{18}F [1,2], and the present system provides a similar testing ground for it. To further progress our understanding of the Be isotopes, we studied the proton-removal spectroscopic factors of the ^{12}B(d, ^{3}He)^{11}Be reaction, and comparisons have been made with the effective-interaction shell model as well as the deformed Nilsson model. Furthermore, the less model-dependent *ab initio* calculations, which aspire to be able to predict rotational band structures in addition to single-particle features in light nuclei, were tested by their descriptions of ^{11}Be, including the new data determined here.

The configurations of low-lying states in ^{11}Be have been extensively studied, indicating quenching of the $N = 8$ shell gap and inversion of the $0p$ and $1s0d$ shells. Although much attention has been paid to the $1/2^+$ halo ground state (g.s.), here, we focus on the negative-parity states. The low-lying negative-parity states have been studied using the ^{9}Be(t, p)^{11}Be reaction [3] and β decay of ^{11}Li [4–6]. These works interpreted the structure of the low-lying negative-parity states within the shell-model framework. The ^{9}Be(^{13}C, ^{11}C)^{11}Be reaction on the well-developed α:n:α structure of ^{9}Be(g.s.) populated the molecular structure of ^{11}Be and suggested a rotational band $K^\pi = 3/2^-$ built on the 3.96-MeV $3/2^-_2$ state, which extends to the $13/2^-$ state [7,8]. Another band is believed to be headed with the relatively bound $1/2^-_1$ state and terminated at the $7/2^-$ state, which is currently the focus of this paper. A summary of the previous studies on ^{11}Be low-lying states can be found in Refs. [9,10].

Studies on ^{12}B have demonstrated the dominance of a $0p$-orbital neutron configuration in its ground state, which has a spin parity of 1^+ [11–13]. With removal of one p-wave proton, the negative-parity states in ^{11}Be are able to be populated. The ^{12}B(d, ^{3}He)^{11}Be reaction can, therefore, be a probe of the neutron p-wave strength in ^{11}Be. The present ^{12}B(d, ^{3}He)^{11}Be reaction solidifies the configuration of the low-lying negative-parity states and determines the strengths within the $0p$-shell orbitals. Negative-parity states with large $\nu(2p\text{-}2h)$ configurations across the $N = 8$ shell gap will not be strongly populated in this reaction, although allowed by the transferred angular momentum. An overall interpretation of

*Present address: National Superconducting Cyclotron Laboratory, East Lansing, Michigan 48824; chenjie@frib.msu.edu
†Present address: Department of Physics, University of Jyvaskyla, FI-40014, Finland.

the low-lying negative-parity states will be presented, which sheds light on the mixing between the $1s0d$ and the $0p$ shells as well as the structures of the $0p$-shell states in ^{11}Be.

II. EXPERIMENT

The ^{12}B$(d,{}^3$He$)^{11}$Be reaction was carried out in inverse kinematics at the ATLAS In-Flight Facility at Argonne National Laboratory. The 12 MeV/u ^{12}B secondary beam was produced using the neutron adding reaction on a ^{11}B primary beam at 13.5 MeV/u. This beam, with an intensity of 200-particle nanoamperes (pnA) bombarded a 3.7-cm-long D_2 gas cell at a pressure of 1400 mbar and temperature of 90 K. The resulting ^{12}B was selected in rigidity by the beamline dipole magnets with a rate of approximately 2×10^5 particles per second and less than 5% contamination. The main contaminant, ^{7}Li^{3+}, had a much lower total energy than the ^{12}B beam and was easily separable in the analysis. Data from ^{11}B$(d,{}^3$He) at 13.5 MeV/u was also collected at the beginning of the experiment and served as an energy calibration and a check of the analysis procedure.

The outgoing charged particles were analyzed by the HELical Orbit Spectrometer (HELIOS) [14,15] with a magnetic-field strength of 2.3 T and an experimental setup resembling that shown in Fig. 2 of Ref. [16]. The ^{12}B ions bombarded a deuterated polyethylene $(CD_2)_n$ target of thickness 400 μg/cm^2 placed within the uniform magnetic field at a position defined as $Z = 0$ cm. The ^{3}He particles from the reaction were transported through the magnetic field to an array of 24 position-sensitive silicon detectors (PSDs) that were positioned downstream of the target covering a range of 72 cm $< Z <$ 107 cm. A group of silicon ΔE-E telescopes were placed at $Z = 42$ cm to identify the $^{9-11}$Be reaction products. The thicknesses of the ΔE and E silicon detectors were $\approx$75 and $\approx$1000 μm, respectively.

The particle identification spectrum from the recoil detectors for the ^{12}B beam bombarding on the CD_2 target appears in Fig. 1. The events in this figure were selected by requiring a 150-ns timing coincidence between a light particle detected in the HELIOS PSD array and a recoil particle detected in the ΔE-E telescope. The energy resolution was sufficient to identify all of the Be isotopes of interest and, thus, discriminate different reaction channels. The corresponding light charged particles with each selected recoil were checked by their cyclotron periods determined from the time-of-flight information between the PSDs and the ΔE-E telescopes.

The ^{11}Be in Fig. 1 were used to discriminate the ^{12}B$(d,{}^3$He) transition to the bound state of ^{11}Be. The ^{10}Be ions, which have a much wider energy distribution, were generated from the transition to the neutron-unbound states of ^{11}Be, which are above the neutron separation energy ($S_n =$ 0.502 MeV) of ^{11}Be. With the energy loss of the escaping neutron, the average energy of ^{10}Be is lower than ^{11}Be. Other possible sources of the ^{10}Be ions in Fig. 1, such as from the ^{12}B$(d,\alpha)^{10}$Be reaction, were essentially excluded because the present setup did not allow detection of the ^{12}B(d,α) reaction to bound states of ^{10}Be.

The incident beam flux was monitored by elastic-scattering events measured on the PSD array. The elastic-scattered

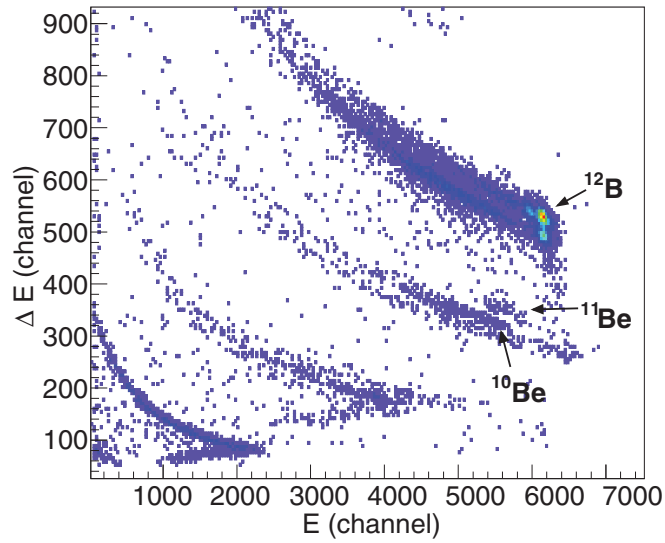

FIG. 1. The ΔE-E spectrum obtained using one of the recoil detector telescopes with ^{12}B incident on the $(CD_2)_n$ target. The data shown required a coincidence with a particle in the PSD array. The particle groups labeled ^{11}Be(^{10}Be) and ^{12}B are from neutron bound (unbound) states in ^{11}Be and the elastic scattering of ^{12}B, respectively.

deuterons on the beam particles were selected by gating on a ^{12}B ion identified in the recoil detectors (see Fig. 1). The deuterons traveling for four cyclotron periods were stopped on the PSDs, and their numbers were used to determine the integrated number of incident particles times the target thickness, the luminosity. Dividing the measured experimental yield (which has been corrected for a solid angle) by the calculated elastic-scattering cross sections gives the luminosity of this measurement. The deuterons were measured at an energy of 3 MeV and at a center-of-mass (c.m.) angle of 23°, and their traveling periods (four times their cyclotron period) were verified by the time-of-flight information. A variety of optical model potentials were used to calculate the elastic-scattering cross section. Uncertainties in the integral of the ^{12}B beam particles times the target thickness varied with a rms of $\approx$30% depending on different optical model parameters. A procedure for determining the absolute yield is described in Sec. IV.

III. RESULTS

The light particles in the PSD array corresponding to the ^{12}B$(d,{}^3$He$)^{11}$Be reaction to the bound or unbound states of ^{11}Be were selected by a coincidence with ^{11}Be or ^{10}Be ions discriminated in the recoil detectors (Fig. 1). Most of the uncorrelated background was removed by using this coincidence. The energies of the light particles selected using this method are plotted in Fig. 2 versus the corresponding distance where the particles were detected by the PSD detectors.

For the present range covered by the PSD array, a clear isolated bound state in ^{11}Be appears as a straight line in the plot of Fig. 2(a). For the unbound states, their loci do not follow straight lines, and different states merge at around $Z = 84$ cm. This is caused by the shallow orbitals of the ^{3}He

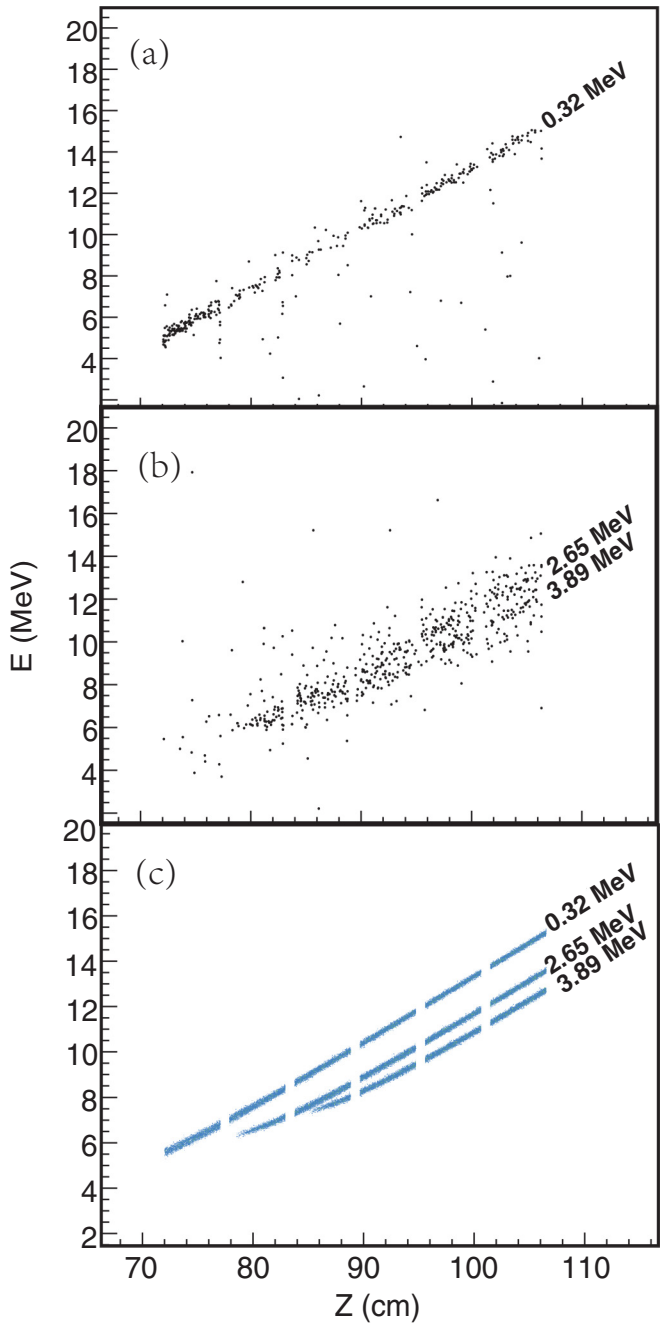

FIG. 2. Measured ^{3}He energies (E) as a function of the distance from the target (Z) for the ^{12}B(d, ^{3}He)^{11}Be reaction in inverse kinematics at 12 MeV/u with a magnetic-field strength of 2.3 T. The data shown required a coincidence with either (a) ^{11}Be or (b) ^{10}Be recoils as shown in Fig. 1. Final states identified in ^{11}Be are labeled by their corresponding excitation energies. (c) The simulation for the different excited states in the ^{12}B(d,^{3} He) reaction. See details in the text.

particles which reached the PSD detectors at radii of $\approx$1.4 cm at shorter distances than the ideal situation. This effect was also observed in the previous (d, ^{3}He) measurement [16]. It is also seen in the Monte Carlo simulation of this reaction with the present setup [see Fig. 2(c)]. Events were selected where

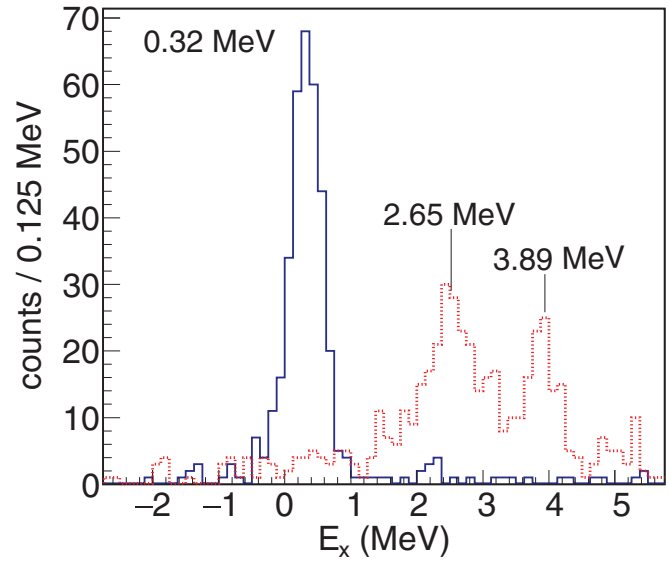

FIG. 3. The excitation-energy spectrum of ^{11}Be neutron bound (blue solid line) and unbound (red dotted line) states determined from the dataset presented in Figs. 2(a) and 2(b), respectively. States identified in the present paper are labeled with their corresponding excitation energies.

the experimental kinematics loci are not merging with each other and were used to obtain the excitation spectrum as well as to evaluate the cross sections for the unbound states. The events ($Z < 85$ cm for the 2.65-MeV state and $Z < 90$ cm for the 3.89-MeV state) which obviously deviate from the straight kinematics lines were not used in the analysis.

Excitation spectra for the ^{12}B(d, ^{3}He) reactions were obtained from the projection of the data along the kinematic lines, and the results are shown in Fig. 3 for both neutron-bound (blue) and -unbound (red) states. The resolution for the excitation-energy spectrum of the bound state is around 560 keV (FWHM), dominated by the properties of the beam, the energy loss, and angle straggling of ^{3}He in the target. The measured widths of the unbound states are also contributed to by their intrinsic widths, which are 228(21) keV for the 2.65-MeV state [3], 3.2(8) keV for the 3.89-MeV state [10], and 7.9(7) keV for the 3.96-MeV states [10]. These widths are also compatible with the present spectrum given the apparent greater width of the 2.65-MeV state.

The peaks in Fig. 3 have been identified with the states reported in the literature for ^{11}Be [17] and are listed in Table I. Below the neutron-separation energy of ^{11}Be, the $1/2^-$ first-excited state at 0.32 MeV was most strongly populated in the ^{12}B(d, ^{3}He) reaction. The unbound $3/2^-_1$ state at 2.654 MeV also presents as a strong transition in the present reaction. The next peak, at 3.89 MeV, probably indicates population of one or both of the states at 3.89 and 3.96 MeV. The relative contribution of these two states is discussed in Sec. VI. The present resolution does not allow separation of the ground state and first-excited state, which are just 320 keV apart. A χ^2 fitting was carried out assuming that both the ground state and the 0.32-MeV state were populated. The best fit

TABLE I. Spectroscopic factors S extracted from the ^{12}B$(d,{}^3$He$)^{11}$Be reaction. The values are normalized such that the sum of S over all transitions is 3.0. Relative uncertainties on S are shown in the parentheses. Details on the uncertainties and the normalization factor are found in the text. Literature energies and spin-parity assignments are from Ref. [17].

Literature		Present data	
E_x (MeV)	J_π	l	S
0.00[a]	$1/2^+$		
0.32	$1/2^-$	$\ell = 1$	0.56(12)
1.78[a]	$5/2^+$		
2.65	$3/2^-$	$\ell = 1$	1.49(44)
3.40[a]	$3/2^{(+,-)}$		
3.89	$5/2^-$	$\ell = 1$	0.95(27)
3.96	$3/2^-$		
5.26[a]	$5/2^-$		
6.71[a]	$(7/2^-)$		

[a]Not observed in the present measurement. See details in the text.

corresponded to a population of the ground state at $<2\%$ of the total events in the 0.32-MeV peak. We place an upper limit on the population of the ground state at 10% of the total events, based on the standard deviation of the χ^2 method. Similarly, in Fig. 3, we cannot rule out some population of the 3.410-MeV state, which was assigned as $3/2^-$ or $3/2^+$ in the previous study [3,4,18]. We place an upper limit on the population of this state at 10% of the total events populated in all combined unbound states. The 5.26-MeV $(5/2^-)$ state is right at the edge of the acceptance of the present setup, so no definite conclusion for its population can be drawn here.

IV. ANGULAR DISTRIBUTIONS

The differential cross sections for each populated state of the ^{12}B$(d,{}^3$He$)^{11}$Be reaction were deduced from the present data using Eq. (4) in Ref. [19]. Every PSD position was either considered as a single center-of-mass angular bin or separated into two bins where the statistics allowed. The center-of-mass angle ($\theta_{\rm c.m.}$) for each bin was determined from the reaction kinematics and the properties of HELIOS within an uncertainty of $\approx 1^\circ$. It is noted that the acceptance of the recoiling ^{10}Be generated from the unbound states of ^{11}Be might decrease due to the breakup process compared to the acceptance of a bound state. The geometrical acceptance of the ^{10}Be ions, generated assuming isotropic decays of the ^{11}Be unbound states, was calculated as a function of c.m. angles and plotted in Fig. 4. Within the range of the present data, the acceptance is mostly above 80%, and it was used to correct the cross sections.

As stated in Sec. II, the total number of incident beam particles multiplied by the target thickness was estimated using the elastic-scattering data measured on the PSD array. Combining this information, the solid angle coverage of the PSDs, and the counts of each state, absolute cross sections were obtained from the present analysis as shown in Fig. 4. Error bars in the figure are statistical only. There is a systematic uncertainty of around 30% for the absolute cross sections which includes

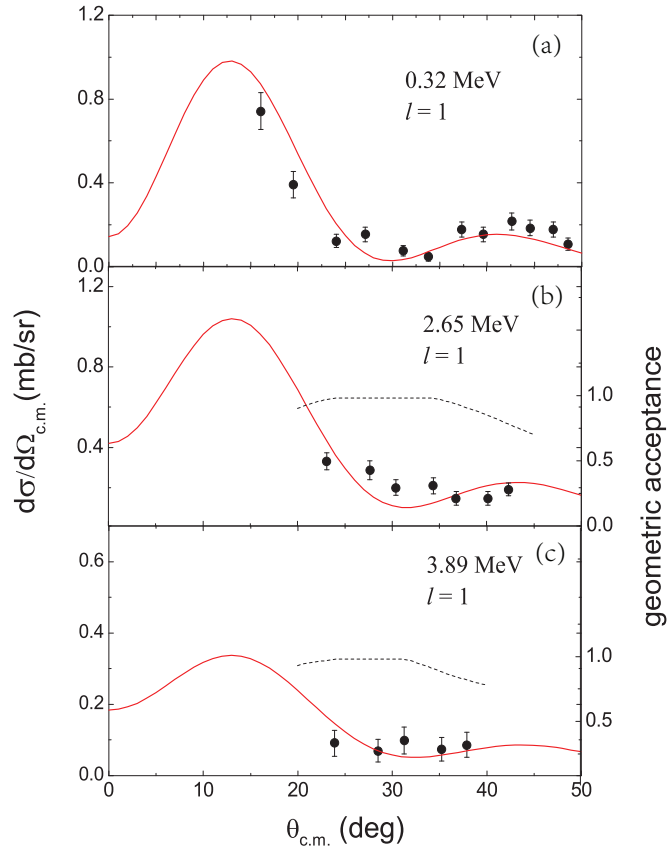

FIG. 4. Experimental (black points) and calculated (red solid lines) angular distributions for the (a) 0.32-, (b) 2.65-, and (c) 3.89-MeV transitions in the ^{12}B$(d,{}^3$He$)^{11}$Be reaction. The curves represent distorted-wave Born 260 approximation (DWBA) calculations for $\ell = 1$ transfer. Only statistical uncertainties are shown for the experimental data, and there is a systematic uncertainty of $\approx 30\%$ on the absolute cross-section scale. The geometrical acceptance of the ^{10}Be recoils for the neutron-unbound states of ^{11}Be is plotted as black dashed curves.

the uncertainties from the determination of the integrated particle number and the cuts on the PID spectrum. Most of the discussions in this paper focus on the relative spectroscopic factor (S), so the uncertainty in the absolute cross sections has very little impact on the conclusions that are drawn based on the present paper.

V. DWBA CALCULATIONS

The spectroscopic factors were extracted from the differential cross sections through a DWBA analysis calculated using the program PTOLEMY [20]. The optical model parameter sets of An and Cai [21] and Pang *et al.* [22] were used as the entrance and exit channels. The Argonne v_{18} [23] potential was used to define the deuteron bound-state wave function and a Woods-Saxon potential with central potential well parameters of $r_0 = 1.25$ and $a_0 = 0.65$ fm, and with spin-orbit parameters of $V_{\rm so} = 6.0$ MeV, $r_{\rm so} = 1.1$, and $a_{\rm so} = 0.65$ fm, was used to define the wave functions of the final proton bound states. The depth of the Woods-Saxon potential well

was adjusted to reproduce the correct binding energy of each of the final proton bound states in ^{11}Be.

The calculated cross sections were normalized to the experimental angular distributions of each populated state using a minimum χ^2 method. The results are presented in Fig. 4. For the 0.32-MeV state, the DWBA calculations with $\ell = 1$ proton transfer reproduce the experimental angular distributions well. The 2.65- and 3.89-MeV state data do not cover the most forward angular-distribution maximum due to the merged trajectories of these unbound states. Since the $\ell = 1$ angular distribution of the 0.32-MeV state is well reproduced by the DWBA calculation, we fit the angular distributions of the 2.65- and 3.89-MeV state for the experimental angular range, and larger uncertainties were determined for these states using various optical model potentials. The extracted spectroscopic factors S are listed in Table I, which have been normalized as described in Sec. VI. For the present reaction, the spectroscopic strengths are simply equivalent to the spectroscopic factors S.

A variety of optical model potentials [21,22,24–28] has been applied to the entrance and exit channels of the DWBA calculations to estimate uncertainties in S. For the relative S, the uncertainties arise from the statistics, the fitting procedure, and variations in the DWBA analysis with the sum of them being $\approx$10% for the 320-keV state and $\approx$20% for the 2.65- and 3.89-MeV states. Different reaction models may bring in an additional 10% uncertainty.

VI. NORMALIZATION OF THE SPECTROSCOPIC STRENGTHS

In the present analysis, the observed p-wave strengths have been normalized to the expected occupancy of the two p orbitals using the Macfarlane and French sum rule [29]. In a simple single-particle picture, the sum of the observed strengths can be normalized to 3, the total number of protons expected to occupy the $0p_{3/2}$ and $0p_{1/2}$ orbitals in ^{12}B. The 0.32-, 2.65-, and 3.89-MeV states were all included in the normalization sum. The strengths from possible higher-lying negative-parity excited states, such as the $5/2^-_2$ state at 5.26 MeV, were assumed to be much smaller than those observed. This assumption was supported by the shell-model calculations discussed in Sec. VII A. This procedure results in a normalization factor of 0.73(26). The large uncertainty comes from the uncertainty in the absolute cross sections and the different optical model potentials.

The entire procedure for the extraction and normalization of the S values was checked using the ^{11}B$(d, ^3$He) data at 13.5 MeV/u taken with the same setup. We have obtained consistent normalized spectroscopic factors (see Sec. VII D) with those reported in Ref. [30] and using the same optical model parameters stated above.

VII. DISCUSSION

In a shell-model picture, states of ^{11}Be should only be strongly populated in the present reaction if doing so corresponds to removal of a p-shell proton from the ground state of ^{12}B. The ground state of ^{12}B is dominated by a p-shell neutron configuration as shown by the neutron-adding and proton-removal reactions [12,13,31]. More specifically, one-proton removal reactions on ^{13}C [11,12,32] indicate the ^{12}B ground state is mostly in the $\pi(0p3/2)^3\nu(0p1/2)^1$ configuration. Thus, states populated in the present reaction are expected to be dominated by a configuration of $\pi(0p_{3/2})^2\nu(0p_{1/2})^1$. Since a pair of protons in the $0p_{3/2}$ orbital can couple to 0^+ or 2^+, the full configuration can carry spin-parity values of $J_\pi = 1/2^-,\ 3/2^-$, or $5/2^-$.

If we consider the low-lying structure of ^{11}Be within the $0p$-$1s0d$ shells (which is reasonable since there is no indication for the intruder of the $1p0f$-shell orbitals), negative-parity states in ^{11}Be are predominantly composed of two major neutron configurations, that is, the configuration within the $0p$-shell orbitals ($0\hbar\omega$), and with two neutrons excited to the $1s0d$ shell ($2\hbar\omega$). The present reaction should selectively populate states with a dominant $0\hbar\omega$ configuration.

There are three major peaks that were strongly populated in this reaction as shown in Fig. 3, corresponding to the $1/2^-_1$ state at 0.32 MeV, the $3/2^-_1$ state at 2.65 MeV, plus one or both of the $5/2^-_1$ states at 3.89 MeV, and the $3/2^-_2$ state at 3.96 MeV. The $1/2^-_1$ state at 0.32 MeV is expected, in a shell-model description, to be dominated by the normal p-shell neutron configuration. This was confirmed by the one-neutron transfer reaction ^{10}Be$(d, p)^{11}$Be [33], which gives a large spectroscopic factor [$S = 0.62(4)$] for the $\ell = 1$ neutron component in this state. The $3/2^-_1$ state at 2.65 MeV was previously seen in the (t, p) reaction [3] and β decay of ^{11}Li [4], suggesting a normal p-shell neutron configuration as well. Our result confirms these observations. The state at 3.889 MeV was previously assigned as $3/2^+$ in the ^{9}Be$(t, p)^{11}$Be reaction measurement [3]. However, the β-delayed decay study [4] revised the spin parity of this state to $5/2^-$. Regarding the likely population of this state in the present measurement, our results are consistent with the $5/2^-$ negative-parity assignment.

There are also some negative-parity states which previous experimental work have indicated to be dominated by configurations with two neutrons excited into the sd shell. The $3/2^-_2$ state is suggested to be dominated by a configuration of $^9\text{Be} \otimes (sd^2)_{(2^+)}$ experimentally (see Table I in Ref. [9]) as well as in the shell-model calculation (see Sec. VII A). The $3/2^-_2$ state at 3.955 MeV should not be strongly populated in the present measurement if there is only a small amount of mixing between the $3/2^-_1$ and the $3/2^-_2$ states. The situation is similar for the $5/2^-_2$ state at 5.26 MeV.

In the following subsections, results with the effective-interaction shell model, Nilsson model, variational Monte Carlo (VMC), and no-core configuration interaction (NCCI) frameworks are compared with experiment. Some of these results are also summarized in Table II and Fig. 5.

A. Shell-model calculations

We have performed shell-model calculations for ^{12}B and ^{11}Be with the recently developed YSOX interaction [34] using the OXBASH code [36]. The calculations assumed ^{4}He as an inert core, and particles could occupy the $0p_{1/2}$, $0p_{3/2}$, $1s_{1/2}$, $0d_{5/2}$, and $0d_{3/2}$ orbitals. The calculated ^{11}Be excitation energies and corresponding spectroscopic

TABLE II. Excitation energies E_x and spectroscopic factors S for the ^{12}B$(d, ^3$He$)^{11}$Be reaction calculated by the shell model using the YSOX [34] interaction, the Nilsson model [35], and the VMC calculations with the AV18 + UX potential [23]. Each set of S values have been normalized to the first-excited state ($1/2^-_1$) state with normalization factors 0.521, 0.5, 0.274, and 0.56(12) for the YOSX interaction, the Nilsson model, the VMC calculation, and the experiment, respectively. The VMC E_x are set relative to the experimental $1/2^+$ energy, and the numbers in parentheses are the Monte Carlo error in the last digit. Also see Fig. 5.

^{11}Be	YSOX		Nilsson		VMC		Experiment	
J_π	E_x (MeV)	S	E_x (MeV)	S	E_x (MeV)	S	E_x (MeV)	S
$1/2^+_1$	0.00	0.003					0.00	
$1/2^-_1$	0.897	1.00	0.125	1.00	0.3(2)	1.00	0.32	1.00(21)
$5/2^+_1$	1.355	0.004					1.78	
$3/2^-_1$	3.091	2.416	2.375	0.8	3.1(4)	1.64	2.65	2.66(79)
$3/2^+_1$	3.994	<0.001					3.41	
$5/2^-_1$	4.918	1.033	3.569	0.2	4.4(4)	0.06	3.89	1.67(48)
$3/2^-_2$	4.636	0.432			5.6(4)	1.47	3.96	
$5/2^-_2$	6.105	<0.001			9.4(4)	0.38	5.26	
$7/2^-_1$	6.671	<0.001			11.2(4)		(6.71)	
$7/2^-_2$	9.365	<0.001	8.875	0.0				

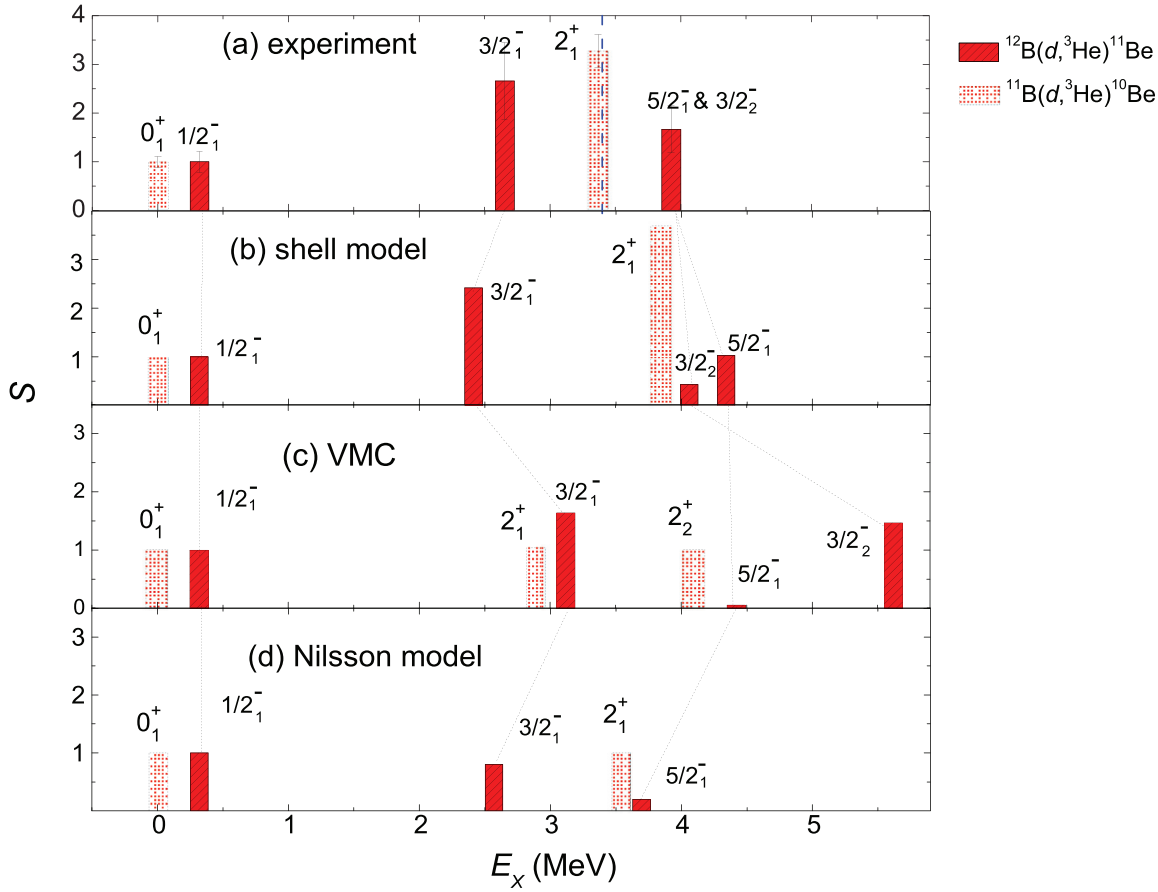

FIG. 5. The (a) experimental and (b)–(d) calculated excitation energies and spectroscopic factors of the $1/2^-_1$, $3/2^-_1$, and $5/2^-_1$ states of ^{11}Be from the ^{12}B$(d, ^3$He$)^{11}$Be reaction (slash bars) and 0^+_1 and 2^+_1 states of ^{10}Be from the ^{11}B$(d, ^3$He$)^{10}$Be reaction (dotted bars). Results shown in panels (b)–(d) were calculated using the shell model with the YSOX interaction [34], the VMC method [23], and the Nilsson model [35], respectively. The error bars for the experimental values are just for relative S. The blue dashed line in (a) is the $(2j + 1)$-weighted energy centroid of $3/2^-_1$ and $5/2^-_1$ states in ^{11}Be. Note that the spectroscopic factors and excitation energies of the first excited state in (a)–(d) were normalized to unity and the experimental value ($E_x = 0.32$ MeV), respectively.

TABLE III. Shell-model occupation numbers for ^{12}B and ^{11}Be with the YSOX interaction.

			Protons				Neutrons					
Nuclide	J_π	E_x (MeV)	$0p_{3/2}$	$0p_{1/2}$	$0d_{5/2}$	$0d_{3/2}$	$0s_{1/2}$	$0p_{3/2}$	$0p_{1/2}$	$0d_{5/2}$	$0d_{3/2}$	$0s_{1/2}$
^{12}B	1^+	0.000	2.701	0.193	0.04	0.052	0.014	3.733	1.117	0.071	0.061	0.018
^{11}Be	$1/2^+_1$	0.000	1.747	0.222	0.009	0.017	0.005	3.459	0.483	0.227	0.04	0.792
	$1/2^-_1$	0.897	1.8	0.162	0.009	0.025	0.005	3.85	1.05	0.05	0.042	0.009
	$5/2^+_1$	1.355	1.71	0.259	0.01	0.017	0.004	3.442	0.502	0.859	0.061	0.137
	$3/2^-_1$	3.091	1.797	0.148	0.015	0.03	0.009	3.374	1.138	0.294	0.061	0.133
	$3/2^+_1$	3.994	1.697	0.269	0.012	0.018	0.005	3.388	0.552	0.244	0.208	0.608
	$3/2^-_2$	4.636	1.658	0.314	0.01	0.015	0.004	2.935	0.545	0.718	0.125	0.677
	$5/2^-_1$	4.918	1.769	0.179	0.019	0.026	0.007	3.788	1.027	0.095	0.055	0.035
	$5/2^-_2$	6.105	1.624	0.356	0.006	0.011	0.003	2.675	0.41	1.032	0.176	0.792
	$7/2^-_1$	6.671	1.629	0.343	0.008	0.016	0.004	2.614	0.418	1.145	0.233	0.59
	$7/2^-_2$	9.365	1.884	0.041	0.029	0.036	0.01	2.919	1.693	0.063	0.239	0.086

factors are given in Table II as well as Fig. 5. Further information about the occupation number of each orbital can be found in Table III. The YSOX interaction reproduces well the ground-state energies, energy levels, electric quadrupole properties, and spin properties for most nuclei in the full *psd* model space including $(0-3)\hbar\omega$ excitations [34]. Comparison is also made with calculations using the WBP interaction [37]. Although the WBP interaction gives the lowest $1/2^-$ and $1/2^+$ states in normal order, the YSOX interaction reproduces the experimentally observed parity inversion, albeit with a larger splitting (0.90 MeV) than observed experimentally (0.32 MeV). We will, therefore, focus on the calculations with the YSOX interaction in the following discussion.

According to the calculations using the YSOX interaction, the spectroscopic factors to all positive-parity states can be neglected ($S < 0.01$) in the ^{12}B$(d, ^3$He$)^{11}$Be reaction. The $1/2^-_1$, $3/2^-_1$, and $5/2^-_1$ states have large overlaps with the ^{12}B g.s., corresponding to the experimentally observed states at 320 keV, 2.654, and 3.899 MeV. These states have a configuration with one particle in the $0p_{1/2}$ orbital and with very little excitation to the *sd* shell, consistent with our previous discussion. The calculated S (Table II) of the former two states are in reasonable agreement with the experimental values. The $3/2^-_2$ state in the calculation probably corresponds to the 3.96-MeV state, and it is dominated by a $2\hbar\omega$ configuration, which has a smaller overlap with the ^{12}B g.s. The S of the $3/2^-_2$ and the $5/2^-_1$ states are added and compared with the experimental spectroscopic factor of the doublet around 3.89 MeV, showing reasonable agreement. If we assume small mixing between the $3/2^-_1$ and the $3/2^-_2$ states, the experimentally observed events at around 3.89 MeV should be dominated by the 3.89-MeV $5/2^-$ state with only a small contribution from the 3.96-MeV $3/2^-_2$ state due to the configuration mixing of the $0\hbar\omega$ excitation.

The maximum angular momentum that can be obtained within the *p*-shell orbitals is $7/2^-$. With a transferred angular momentum of $\ell = 1$, the present reaction cannot populate states of this angular momentum. Nonetheless, we list the shell-model calculations for the first two $7/2^-$ states in Tables II and III for comparison. There is no firmly assigned experimental $7/2^-$ state in the literature [17].

There is a $5/2^-_2$ state at around 6 MeV in the calculation with a $2\hbar\omega$ configuration which could naturally be identified with the previously observed 5.255-MeV state in the ^{9}Be(t, p) reaction [3]. This state could not be observed in the present measurement due to the acceptance of the setup. However, the calculated spectroscopic factor for this state is much smaller than the $5/2^-_1$ state or the $3/2^-_1$ states, indicating the *p*-wave strength observed in this measurement could account for most of the proton-removal strengths. This suggests that it is reasonable to normalize the sum of them to the occupancy of the *p*-wave orbital in the ^{12}B g.s., as performed in Sec. VI.

B. Nilsson model calculations

The strong α clustering in ^{8}Be naturally suggests that deformation degrees of freedom will play an important role on the structure of the Be isotopes, a topic that has been extensively discussed in the literature (see Ref. [38] for a review). The deformation in ^{8}Be is evidenced by the ground-state rotational band and the enhanced $E2$ transition [39]. Furthermore, Bohr and Mottelson [40] proposed the effects of deformation to explain the inversion of the $1/2^+$ and the $1/2^-$ states.

Here, we attempt to describe the spectroscopic factors data in terms of the Nilsson model in the strong-coupling limit. Within this framework, the $K = 1/2^-$ can be associated with the neutron 1/2[220] level. The excitation energies follow:

$$E_x(J) = E_0 + \frac{\hbar^2}{2\Theta}[J(J+1) + a(-)^{J+1/2}(J+1/2)], \quad (1)$$

with the rotational parameter $b = \hbar/2\Theta = 0.5$ MeV and a decoupling parameter $a = 0.5$ in line with Nilsson calculations for deformations of 0.3 to 0.4. This band is expected to be terminated by the $7/2^-$ state with all the angular momenta of the valence nucleons aligned. It appears that the second $7/2^-$ state in Tables II and III belongs to this band due to its dominant configuration within the *p* shell.

For $Z = 5$, the last proton is expected to occupy the 3/2[101] level, and the g.s. of ^{12}B is the bandhead of the $K = 1$ band originating from the coupling of the two Nilsson levels above. Since the level parentage is attributed only to

the $0p_{3/2}$ orbit, the spectroscopic factors depend only on the Clebsch-Gordan coefficients according to Eq. (3) of Ref. [35], and we predict S as listed in Table II and shown in Fig. 5. The spectroscopic factors of the $3/2^-_1$ and $5/2^-_1$ states were underestimated in this framework, perhaps suggesting deviations (due to Coriolis coupling) from the strong-coupling limit for the odd-odd ^{12}B $K = 1$ band that should be explored.

C. *Ab initio* theory

Ab initio nuclear theory sets out to predict nuclear properties starting directly from the description of the nucleus as a system of interacting nucleons [41–50]. The aim is to provide a predictive theory which removes the simplifying assumptions of phenomenological approaches and ties the predictions for the many-body system directly to our understanding of the internucleon interactions [23,51,52]. In the following, we present two sets of *ab initio* calculations that use realistic interactions fit to *NN* elastic-scattering data: VMC and NCCI.

1. Variational Monte Carlo calculations

The VMC calculations begin with the construction of correlated wave-functions $\Psi(J^\pi, T, T_z)$ for the nuclei of interest as approximate solutions of the nonrelativistic Schrödinger equation $H\Psi = E\Psi$. In the present paper, we use the Argonne v_{18} two-nucleon and Urbana X three-nucleon potentials (AV18 + UX) for our Hamiltonian. The wave functions are constructed from products of two- and three-body correlation operators acting on an antisymmetric single-particle state of the appropriate quantum numbers. The correlation operators are designed to reflect the influence of the two- and three-nucleon potentials at short distances, whereas appropriate boundary conditions are imposed at long range. The $\Psi(J^\pi, T, T_z)$ have embedded variational parameters that are adjusted to minimize the energy expectation value,

$$E_V = \frac{\langle\Psi|H|\Psi\rangle}{\langle\Psi|\Psi\rangle} \geqslant E_0, \tag{2}$$

which is evaluated by Metropolis Monte Carlo integration. The VMC wave functions serve as the starting point for the exact Green's function Monte Carlo (GFMC) calculations, which have been very successful in reproducing energies, electromagnetic moments, and transition rates in light nuclei up to ^{12}C. However, GFMC calculations have not yet been performed for the ^{11}Be and ^{12}B nuclei studied here. A comprehensive review of the VMC and GFMC methods is given in Ref. [50].

For the negative-parity states in ^{11}Be the single-particle state is constructed in *LS* coupling with all possible [4421] and [4331] spatial symmetries within the p shell as specified in Young diagram notation, including 2P, 2D, 2F[4421], and 2S, 4S, 2D, and 4D[4421] components. The relative strengths of these components are obtained in a small-basis diagonalization after all the correlations have been applied. The first six negative-parity states are $1/2^-$, $3/2^-$, $5/2^-$, $3/2^-$, $5/2^-$, and $7/2^-$ as shown in Table II, in agreement with the observed experimental ordering, although with a greater spread in excitation energies. The unnatural parity $1/2^+$ ground state has not yet been evaluated, so the excitation energies shown assume a 0.3-MeV starting point for the $1/2^-$ state.

The low-lying states in ^{12}B are constructed starting from single-particle states with all possible [4431] spatial symmetries within the p shell, including 3P, 3D, 3F, 1P, and 1D components. After the small-basis diagonalization, we find considerable degeneracy among the low-lying states with two 1^+ levels and a 2^+ level all in close proximity. Although this is not an entirely satisfactory status, for the present purpose, we identify the 1^+ state that has positive magnetic and quadrupole moments as the ground state and use it to evaluate the spectroscopic overlaps with ^{11}Be, following the method discussed in Ref. [53]. The absolute spectroscopic factors obtained are significantly quenched relative to the nominal occupation of three protons in ^{12}B, but the relative spectroscopic factors given in Table II and Fig. 5 are normalized to the first excited state ($1/2^-_1$) as for the other calculations.

Compared to the experimental values, the VMC calculation presents a correct level order for the low-lying negative-parity states, but the energy difference of the $3/2^-_2$ and $5/2^-_1$ is much larger than the experimental values. The calculated spectroscopic factors show a reasonable agreement with the experiment. Compared to the shell-model calculation, the spectroscopic factor of the $3/2^-_2$ state is much larger than the $5/2^-_1$ state, indicating larger mixing of the $0\hbar\omega$ and $2\hbar\omega$ configurations in this calculation.

2. No-core configuration interaction calculations

Here, we examine the extent to which *ab initio* NCCI calculations predict a low-lying spectrum for ^{11}Be consistent with that experimentally observed in ^{11}Be. We focus on the negative-parity states and use the Daejeon16 nucleon-nucleon interaction [54]. These calculations, presented in further detail in Ref. [55], are carried out with the NCCI code MFDN [56–58].

In the NCCI, or no-core shell model, approach [48], the many-body Schrödinger equation is solved in a basis of Slater determinants (antisymmetrized products) of harmonic-oscillator orbitals. In practice, this basis must be truncated, generally at some maximum number $N_{\max}$ of oscillator excitations. The results converge, a $N_{\max} \to \infty$, towards the solution to the original untruncated Schrödinger equation problem. The accuracy of this solution is constrained by available computational resources and, thus, maximum accessible $N_{\max}$ for the basis. We must verify that any calculation at finite $N_{\max}$ yields sufficiently accurate (or converged) results to permit meaningful comparison of observables with experiment (e.g., Refs. [59–62]).

The low-lying negative-parity spectrum for ^{11}Be, calculated with a basis truncation of $N_{\max} = 10$ (and a basis oscillator parameter of $\hbar\omega = 15$ MeV) is shown in Fig. 6(a). Although the absolute (or binding) energies are not well converged in the calculation (they change by an MeV or more between the $N_{\max} = 8$ and 10 calculations), many of the features of the low-lying *excitation* spectrum, or *relative* energies between states, are, in fact, much more robustly converged in the calculations. In general, the low-lying rotational band structure emerges at comparatively low $N_{\max}$ in

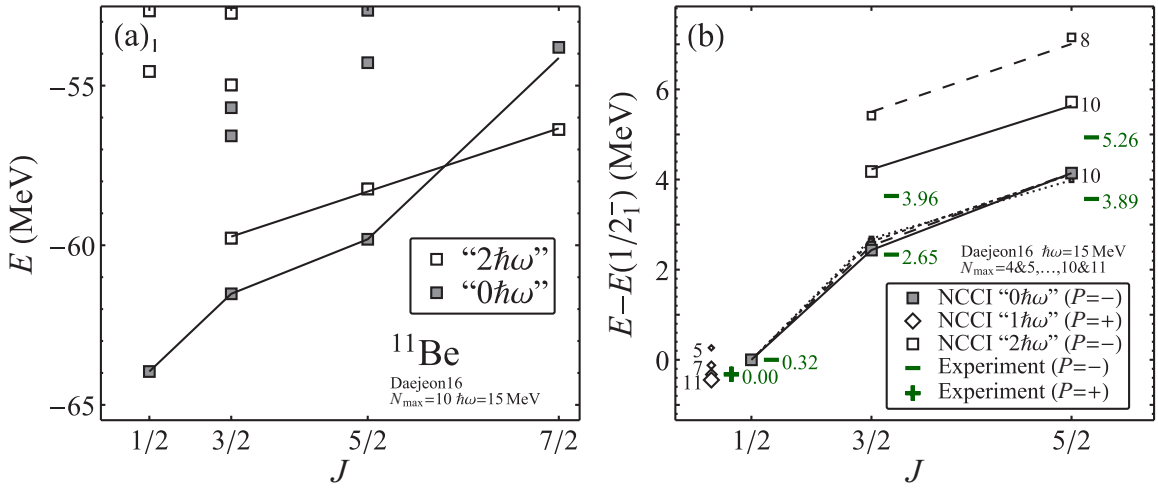

FIG. 6. *Ab initio* NCCI calculated energy spectrum for negative-parity states of ^{11}Be with the Daejeon16 interaction. Energies are plotted against an angular momentum axis scaled as $J(J+1)$ as appropriate for rotational analysis. (a) Calculated negative-parity spectrum ($N_{\max} = 10$, $\hbar\omega = 15$ MeV), shown with fits of the rotational energy formula (1) to the calculated band member energies (lines). States are classified as $0\hbar\omega$ (shaded square) or "$2\hbar\omega$" (open squares) as described in the text. (b) Calculated *relative* energies, taken with respect to the $1/2^-_1$ ground state of the negative-parity space. These are shown for successively larger bases as indicated by increasing symbol size from $N_{\max} = 4$ (dotted line) through 10 (solid line). The relative energy of the calculated $1/2^+_1$ is also shown (diamonds) from $N_{\max} = 5$ through 11. Energies for the experimental counterparts are shown (− for negative parity or + for positive parity) for comparison (these are labeled with the experimental excitation energies in MeV for convenient identification).

NCCI calculations of the Be isotopes [55,63–65]. Rotational energy fits to the lowest negative-parity band ($K^P = 1/2^-$) and excited negative-parity band ($K^P = 3/2^-$) are shown in Fig. 6(a).

The relative energies of the members of the lowest negative-parity band from the NCCI calculations are shown in Fig. 6(b). The calculated relative energies within the $K^P = 1/2^-$ band are comparatively independent of $N_{\max}$, varying by less than $\approx$0.1 MeV, at $N_{\max} = 10$. Comparing with experiment [dashes in Fig. 6(b)], the NCCI prediction for the relative energy of the $3/2^-$ and $1/2^-$ band members is consistent with experiment to within $\approx$0.1 MeV. The $5/2^-$ assignment for the state at 3.89 MeV places the *ab initio* calculated and experimental values for the relative energy of the $3/2^-$ and $1/2^-$ band members in agreement to within $\approx$0.6 MeV.

To place these negative-parity states in the context of the positive-parity ground state, we also show the energy of the $1/2^+_1$ state relative to the $1/2^-_1$ in Fig. 6(b). Although this energy difference is not quite as well converged with $N_{\max}$ as those between the negative-parity band members, it is already apparent that the Daejeon16 interaction reproduces (and, in fact, somewhat overestimates) the experimentally observed parity inversion [66,67].

However, the calculated excitation energy of the excited $K^P = 3/2^-$ band, relative to the $1/2^-_1$ state, is still highly sensitive to the basis truncation. Although the calculated energies are decreasing towards the experimental values with increasing $N_{\max}$ [Fig. 6(b)], it is not yet possible to reliably estimate what the converged values might be and to make a meaningful comparison.

At a qualitative level, the low-lying states obtained in the present NCCI calculation for ^{11}Be may be classified into $0\hbar\omega$ and $2\hbar\omega$ states as indicated in Fig. 6(a) (by the shaded and open symbols, respectively), based on their calculated wave functions. Taking the $5/2^-_1$ and $5/2^-_2$ states for illustration, in Fig. 7, we examine the contributions to the norm (or probability) coming from oscillator configurations with $N_{\rm ex} = 0, 2, 4, \ldots$ excitation quanta relative to the lowest permitted filling of oscillator shells, i.e., the $0\hbar\omega$, $2\hbar\omega$, etc., components of the wave function. For the $5/2^-_1$ state [Fig. 7(b)], the contribution from $0\hbar\omega$ oscillator configurations dominates (although some of this probability bleeds off to higher $N_{\rm ex}$ contributions as $N_{\max}$ increases). In contrast, for the $5/2^-_2$ state [Fig. 7(a)], the $0\hbar\omega$ contribution is highly suppressed with the largest contribution coming from $2\hbar\omega$ and then falling off gradually for higher $N_{\rm ex}$. In this sense, the NCCI calculations suggest a $0\hbar\omega$ character for the $K^P = 1/2^-$ band members ($1/2^-_1$, $3/2^-_1$, $5/2^-_1, \ldots$) and a $2\hbar\omega$ character for the $K^P = 3/2^-$ band members ($3/2^-_2$, $5/2^-_2, \ldots$).

D. Comparisons with ^{11}B(d, ^{3}He)^{10}Be data

The ^{11}B(d, ^{3}He)^{10}Be reaction also serves as a testing ground for the different theoretical models. Information could be obtained from previous data as well as the stable beam data in the present experiment. The present measurement gives spectroscopic factors of 0.61(6), 2.09(21), and 0.30(6) for the g.s. (0^+), 2^+_1, and 2^+_2 states, which is consistent with the previous measurement [30]. In order to further understand the experimental results, we also compare the experimental spectroscopic factors of the ^{11}B(d, ^{3}He)^{10}Be reaction to the calculated ones of the shell model using the YSOX interaction, the Nilsson model, and the VMC calculation. Figure 5 represents these calculated spectroscopic factors and excitation energies in comparison with the experiments for the $1/2^-_1$, $3/2^-_1$, $5/2^-_1$ states of ^{11}Be in the ^{12}B(d,^{3}He)^{11}Be

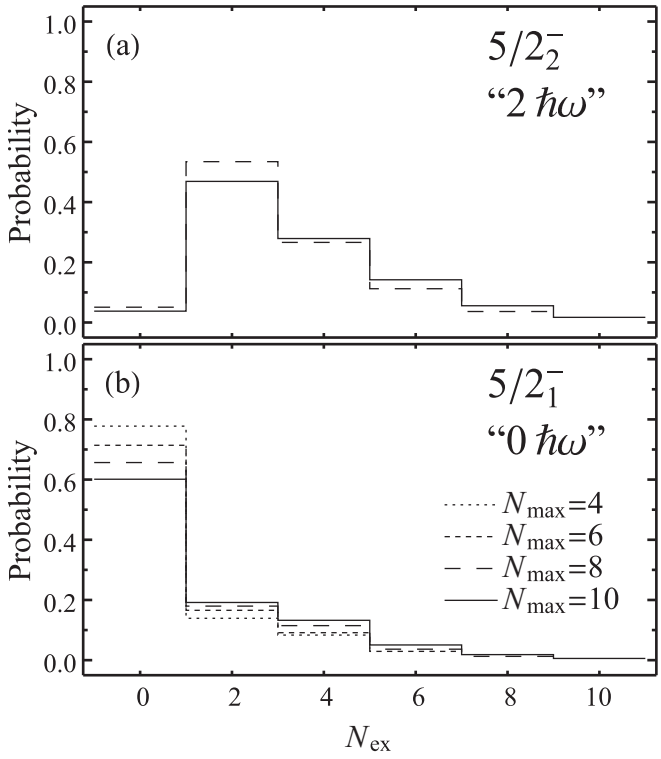

FIG. 7. Decomposition of NCCI calculated eigenstates for the (a) $5/2_2^-$ and (b) $5/2_1^-$ states with respect to the number of excitation quanta N_{ex} in the contributing oscillator configurations. These decompositions are for the same calculations as shown in Fig. 6(b) with the histograms overlaid for $N_{max} = 4$ (dotted line) through 10 (solid line).

reaction and 0_1^+ and 2_1^+ states of ^{10}Be in the ^{11}B$(d, ^3$He$)^{10}$Be reaction. The excitation energy of the 2^+ state of ^{10}Be in the Nilsson model was calculated using $b = 0.59$. It is noted that the calculated excitation energies of the $1/2^-$ state were all normalized to the experimental value, and its spectroscopic factors were normalized to unity in order to compare the relative excitation energies and spectroscopic factors of the negative-parity states in these different calculations on equal footing.

Experimental and theoretical studies hinted on the existence of $N = 6$ subshell closures in ^{8}He [68] and ^{14}O [69,70]. More recently, various sides of evidence for the $Z = 6$ shell closure in $^{13-20}$C has been reported [71]. If we assume that $N = 6$ is a robust subshell, the $1/2_1^-$, $3/2_1^-$, and $5/2_1^-$ states could be viewed as composed of one neutron in $0p_{1/2}$ orbital outside the ^{10}Be(0^+) or ^{10}Be(2^+) core. The $(2j + 1)$-weighted energy centroid of $3/2_1^-$ and $5/2_1^-$ states (shown as the dashed red line in Fig. 5) compared to the $1/2_1^-$ state in ^{11}Be is close to the energy difference of the 2_1^+ and 0_1^+ states in ^{10}Be. Furthermore, the spectroscopic factors of the $1/2_1^-$ state and the sum of $3/2_1^-$ and $5/2_1^-$ states are close to the values of the 0_1^+ and 2_1^+ states for the ^{11,12}B$(d, ^3$He$)$ transitions, respectively (see Fig. 5). The spectroscopic study of the negative-parity states populated in the proton-removal reactions on ^{11,12}B show a consistent picture with the valence neutron in the $0p_{1/2}$ orbital coupling to the ^{10}Be core.

VIII. SUMMARY

Single-particle overlaps between negative-parity states in ^{11}Be and the ground state of ^{12}B have been determined from the measured cross sections of the ^{12}B$(d, ^3$He$)^{11}$Be reaction at 12 MeV/u in inverse kinematics. Spectroscopic factors were extracted from a DWBA analysis and compared with various theoretical calculations from the shell model, Nilsson model, and *ab initio* methods. Considering the dominant *p*-wave neutron configuration in the ^{12}B ground state, the strong population of certain low-lying negative-parity states in ^{11}Be indicates the dominant neutron *p*-wave configuration of these states.

Shell-model calculations using the YSOX effective interaction reproduce the spectroscopic factors of the low-lying negative-parity states and their excitation energies relative to the $1/2_1^-$ state, but the level orders of the $5/2_1^-$ and $3/2_1^-$ states are inverted with respect to experiment. The VMC calculation presents a correct level ordering although it suggests far larger mixing between excited $3/2^-$ levels. The calculations using the Nilsson model framework underestimate the spectroscopic factors of $3/2_1^-$ and $5/2_1^-$ states. The NCCI calculation reproduces the dominant oscillator configurations as well as the relative excitation energies of these states.

ACKNOWLEDGMENTS

The authors would like to acknowledge the hard work of the support and operations staff at ATLAS. We thank J. P. Schiffer and P. J. Fasano for valuable discussions. This research used resources of Argonne National Laboratory's ATLAS facility, which is a Department of Energy Office of Science User Facility. This material is based upon work supported by the US Department of Energy, Office of Science, Office of Nuclear Physics, under Contract No. DE-AC02-06CH11357 (ANL) and Grants No. DE-FG02-96ER40978 (LSU), No. DE-FG02-95ER-40934 (ND), No. DE-SC0014552 (UConn), No. DE-AC02-05CH11231(LBNL), and No. DE-SC0009971 (CUSTIPEN). J.C. acknowledges partial support by the FRIB-CSC Fellowship under Grant No. 201600090345. C.X.Y. and Y.L.Y. acknowledge the National Natural Science Foundation of China Grants No. 11775316, No. 11535004, and No. 11875074. This research used computational resources of the National Energy Research Scientific Computing Center (NERSC), a US Department of Energy, Office of Science, user facility supported under Contract No. DE-AC02-05CH11231, and of the Argonne Laboratory Computing Resource Center; support from the NUCLEI SciDAC program is gratefully acknowledged. We gratefully acknowledge use of the Bebop cluster in the Laboratory Computing Resource Center at Argonne National Laboratory.

[1] D. Santiago-Gonzalez, K. Auranen, M. L. Avila, A. D. Ayangeakaa, B. B. Back, S. Bottoni, M. P. Carpenter, J. Chen, C. M. Deibel, A. A. Hood, C. R. Hoffman, R. V. F. Janssens, C. L. Jiang, B. P. Kay, S. A. Kuvin, A. Lauer, J. P. Schiffer, J. Sethi, R. Talwar, I. Wiedenhöver, J. Winkelbauer, and S. Zhu, Phys. Rev. Lett. **120**, 122503 (2018).

[2] A. O. Macchiavelli *et al.* (unpublished).

[3] G.-B. Liu and H. T. Fortune, Phys. Rev. C **42**, 167 (1990).

[4] Y. Hirayama, T. Shimoda, H. Izumi, A. Hatakeyama, K. Jackson, C. Levy, H. Miyatake, M. Yagi, and H. Yano, Phys. Lett. B **611**, 239 (2005).

[5] D. Morrissey, K. McDonald, D. Bazin, B. Brown, R. Harkewicz, N. Orr, B. Sherrill, G. Souliotis, M. Steiner, J. Winger, S. Yennello, B. Young, S. Lukyanov, G. Chubarian, and Y. Oganessian, Nucl. Phys. A **627**, 222 (1997).

[6] N. Aoi, K. Yoneda, H. Miyatake, H. Ogawa, Y. Yamamoto, E. Ideguchi, T. Kishida, T. Nakamura, M. Notani, H. Sakurai, T. Teranishi, H. Wu, S. Yamamoto, Y. Watanabe, A. Yoshida, and M. Ishihara, Nucl. Phys. A **616**, 181 (1997).

[7] H. Bohlen, R. Kalpakchieva, W. von Oertzen, T. Massey, B. Gebauer, S. Grimes, T. Kokalova, H. Lenske, A. Lenz, M. Milin, C. Schulz, S. Thummerer, S. Torilov, and A. Tumino, Nucl. Phys. A **722**, C3 (2003).

[8] H. G. Bohlen, W. von Oertzen, R. Kalpakchieva, T. N. Massey, T. Dorsch, M. Milin, C. Schulz, T. Kokalova, and C. Wheldon, J. Phys.: Conf. Ser. **111**, 012021 (2008).

[9] H. T. Fortune and R. Sherr, Phys. Rev. C **83**, 054314 (2011).

[10] H. T. Fortune, Phys. Rev. C **86**, 037302 (2012).

[11] G. Mairle and G. Wagner, Nucl. Phys. A **253**, 253 (1975).

[12] J. Lind, G. Garvey, and R. Tribble, Nucl. Phys. A **276**, 25 (1977).

[13] H. Y. Lee, J. P. Greene, C. L. Jiang, R. C. Pardo, K. E. Rehm, J. P. Schiffer, A. H. Wuosmaa, N. J. Goodman, J. C. Lighthall, S. T. Marley, K. Otsuki, N. Patel, M. Beard, M. Notani, and X. D. Tang, Phys. Rev. C **81**, 015802 (2010).

[14] A. Wuosmaa, J. Schiffer, B. Back, C. Lister, and K. Rehm, Nucl. Instrum. Methods Phys. Res., Sect. A **580**, 1290 (2007).

[15] J. Lighthall, B. Back, S. Baker, S. Freeman, H. Lee, B. Kay, S. Marley, K. Rehm, J. Rohrer, J. Schiffer, D. Shetty, A. Vann, J. Winkelbauer, and A. Wuosmaa, Nucl. Instrum. Methods Phys. Res., Sect. A **622**, 97 (2010).

[16] S. Bedoor, A. H. Wuosmaa, M. Albers, M. Alcorta, S. Almaraz-Calderon, B. B. Back, P. F. Bertone, C. M. Deibel, C. R. Hoffman, J. C. Lighthall, S. T. Marley, D. G. Mcneel, R. C. Pardo, K. E. Rehm, J. P. Schiffer, and D. V. Shetty, Phys. Rev. C **93**, 044323 (2016).

[17] J. Kelley, E. Kwan, J. Purcell, C. Sheu, and H. Weller, Nucl. Phys. A **880**, 88 (2012).

[18] N. Fukuda, T. Nakamura, N. Aoi, N. Imai, M. Ishihara, T. Kobayashi, H. Iwasaki, T. Kubo, A. Mengoni, M. Notani, H. Otsu, H. Sakurai, S. Shimoura, T. Teranishi, Y. X. Watanabe, and K. Yoneda, Phys. Rev. C **70**, 054606 (2004).

[19] C. R. Hoffman, B. B. Back, B. P. Kay, J. P. Schiffer, M. Alcorta, S. I. Baker, S. Bedoor, P. F. Bertone, J. A. Clark, C. M. Deibel, B. DiGiovine, S. J. Freeman, J. P. Greene, J. C. Lighthall, S. T. Marley, R. C. Pardo, K. E. Rehm, A. Rojas, D. Santiago-Gonzalez, D. K. Sharp, D. V. Shetty, J. S. Thomas, I. Wiedenhöver, and A. H. Wuosmaa, Phys. Rev. C **85**, 054318 (2012).

[20] M. H. Macfarlane and S. C. Pieper, Argonne National Laboratory Report No. ANL-76-11, Rev. 1, 1978 (unpublished).

[21] H. An and C. Cai, Phys. Rev. C **73**, 054605 (2006).

[22] D. Y. Pang, P. Roussel-Chomaz, H. Savajols, R. L. Varner, and R. Wolski, Phys. Rev. C **79**, 024615 (2009).

[23] R. B. Wiringa, V. G. J. Stoks, and R. Schiavilla, Phys. Rev. C **51**, 38 (1995).

[24] Y. Han, Y. Shi, and Q. Shen, Phys. Rev. C **74**, 044615 (2006).

[25] W. W. Daehnick, J. D. Childs, and Z. Vrcelj, Phys. Rev. C **21**, 2253 (1980).

[26] R. Varner, W. Thompson, T. McAbee, E. Ludwig, and T. Clegg, Phys. Rep. **201**, 57 (1991).

[27] J. Lohr and W. Haeberli, Nucl. Phys. A **232**, 381 (1974).

[28] C.-T. Liang, X.-H. Li, and C.-H. Cai, J. Phys. G: Nucl. Part. Phys. **36**, 085104 (2009).

[29] M. H. Macfarlane and J. B. French, Rev. Mod. Phys. **32**, 567 (1960).

[30] U. Schwinn, G. Mairle, G. J. Wagner, and C. Rämer, Z. Phys. A: At. Nucl. **275**, 241 (1975).

[31] G. Mairle, L. K. Pao, G. J. Wagner, K. T. Knöpfle, and H. Riedesel, Z. Phys. A: At. Nucl. **301**, 157 (1981).

[32] D. Scott, P. Portner, J. Nelson, A. Shotter, A. Mitchell, N. Chant, D. Montague, and K. Ramavataram, Nucl. Phys. A **141**, 497 (1970).

[33] K. T. Schmitt, K. L. Jones, A. Bey, S. H. Ahn, D. W. Bardayan, J. C. Blackmon, S. M. Brown, K. Y. Chae, K. A. Chipps, J. A. Cizewski, K. I. Hahn, J. J. Kolata, R. L. Kozub, J. F. Liang, C. Matei, M. Matoš, D. Matyas, B. Moazen, C. Nesaraja, F. M. Nunes, P. D. O'Malley, S. D. Pain, W. A. Peters, S. T. Pittman, A. Roberts, D. Shapira, J. F. Shriner, M. S. Smith, I. Spassova, D. W. Stracener, A. N. Villano, and G. L. Wilson, Phys. Rev. Lett. **108**, 192701 (2012).

[34] C. Yuan, T. Suzuki, T. Otsuka, F. Xu, and N. Tsunoda, Phys. Rev. C **85**, 064324 (2012).

[35] A. O. Macchiavelli, H. L. Crawford, C. M. Campbell, R. M. Clark, M. Cromaz, P. Fallon, M. D. Jones, I. Y. Lee, and M. Salathe, Phys. Rev. C **97**, 011302(R) (2018).

[36] B. A. Brown, A. Etchegoyen, N. S. Godwin, W. Rae, W. D.M. Richter, W. Ormand, E. Warburton, J. Winfield, L. Zhao, and C. H. Zimmerman, Oxbash for Windows, Report MSU NSCL Report No. 1289, 2004 (unpublished).

[37] E. K. Warburton and B. A. Brown, Phys. Rev. C **46**, 923 (1992).

[38] W. von Oertzen, M. Freer, and Y. Kanada-En'yo, Phys. Rep. **432**, 43 (2006).

[39] V. M. Datar, S. Kumar, D. R. Chakrabarty, V. Nanal, E. T. Mirgule, A. Mitra, and H. H. Oza, Phys. Rev. Lett. **94**, 122502 (2005).

[40] A. Bohr and B. R. Mottelson, *Nuclear Structure, Vol. II: Nuclear Deformations* (World Scientific, Singapore, 1998), p. 33.

[41] P. Navrátil, J. P. Vary, and B. R. Barrett, Phys. Rev. Lett. **84**, 5728 (2000).

[42] T. Neff and H. Feldmeier, Nucl. Phys. A **738**, 357 (2004).

[43] G. Hagen, D. J. Dean, M. Hjorth-Jensen, T. Papenbrock, and A. Schwenk, Phys. Rev. C **76**, 044305 (2007).

[44] S. Quaglioni and P. Navrátil, Phys. Rev. C **79**, 044606 (2009).

[45] S. Bacca, N. Barnea, and A. Schwenk, Phys. Rev. C **86**, 034321 (2012).

[46] N. Shimizu, T. Abe, Y. Tsunoda, Y. Utsuno, T. Yoshida, T. Mizusaki, M. Honma, and T. Otsuka, Prog. Exp. Theor. Phys. **2012**, 01A205.

[47] T. Dytrych, K. D. Launey, J. P. Draayer, P. Maris, J. P. Vary, E. Saule, U. Catalyurek, M. Sosonkina, D. Langr, and M. A. Caprio, Phys. Rev. Lett. **111**, 252501 (2013).

[48] B. R. Barrett, P. Navrátil, and J. P. Vary, Prog. Part. Nucl. Phys. **69**, 131 (2013).
[49] S. Baroni, P. Navrátil, and S. Quaglioni, Phys. Rev. C **87**, 034326 (2013).
[50] J. Carlson, S. Gandolfi, F. Pederiva, S. C. Pieper, R. Schiavilla, K. E. Schmidt, and R. B. Wiringa, Rev. Mod. Phys. **87**, 1067 (2015).
[51] D. R. Entem and R. Machleidt, Phys. Rev. C **68**, 041001(R) (2003).
[52] E. Epelbaum, H.-W. Hammer, and U.-G. Meißner, Rev. Mod. Phys. **81**, 1773 (2009).
[53] I. Brida, S. C. Pieper, and R. B. Wiringa, Phys. Rev. C **84**, 024319 (2011).
[54] A. M. Shirokov, I. J. Shin, Y. Kim, M. Sosonkina, P. Maris, and J. P. Vary, Phys. Lett. B **761**, 87 (2016).
[55] M. A. Caprio, P. J. Fasano, J. P. Vary, P. Maris, and J. Hartley, in *Proceedings of the International Conference Nuclear Theory in the Supercomputing Era 2018*, edited by A. M. Shirokov and A. I. Mazur (Pacific National University, Khabarovsk, Russia), arXiv:1909.13417.
[56] P. Maris, M. Sosonkina, J. P. Vary, E. Ng, and C. Yang, Procedia Comput. Sci. **1**, 97 (2010).
[57] H. M. Aktulga, C. Yang, E. G. Ng, P. Maris, and J. P. Vary, Concurrency Computat.: Pract. Exper. **26**, 2631 (2013).
[58] M. Shao, H. M. Aktulga, C. Yang, E. G. Ng, P. Maris, and J. P. Vary, Comput. Phys. Commun. **222**, 1 (2018).
[59] S. K. Bogner, R. J. Furnstahl, P. Maris, R. J. Perry, A. Schwenk, and J. Vary, Nucl. Phys. A **801**, 21 (2008).
[60] P. Maris, J. P. Vary, and A. M. Shirokov, Phys. Rev. C **79**, 014308 (2009).
[61] P. Maris and J. P. Vary, Int. J. Mod. Phys. E **22**, 1330016 (2013).
[62] S. L. Henderson, T. Ahn, M. A. Caprio, P. J. Fasano, A. Simon, W. Tan, P. O'Malley, J. Allen, D. W. Bardayan, D. Blankstein, B. Frentz, M. R. Hall, J. J. Kolata, A. E. McCoy, S. Moylan, C. S. Reingold, S. Y. Strauss, and R. O. Torres-Isea, Phys. Rev. C **99**, 064320 (2019).
[63] P. Maris, M. A. Caprio, and J. P. Vary, Phys. Rev. C **91**, 014310 (2015); **99**, 029902(E) (2019).
[64] M. A. Caprio, P. Maris, J. P. Vary, and R. Smith, Int. J. Mod. Phys. E **24**, 1541002 (2015).
[65] M. A. Caprio *et al.* (unpublished).
[66] A. M. Shirokov, I. J. Shin, Y. Kim, M. Sosonkina, P. Maris, and J. P. Vary, *Book of Abstracts of the XXII International Conference on Few-Body Problems in Physics (FB22), Caen, France, 2018* (Springer, Berlin, 2018).
[67] Y. Kim, I. J. Shin, A. M. Shirokov, M. Sosonkina, P. Maris, and J. P. Vary, in *Proceedings of the International Conference Nuclear Theory in the Supercomputing Era 2018*, edited by A. M. Shirokov and A. I. Mazur (Pacific National University, Khabarovsk, Russia), arXiv:1910.04367.
[68] F. Skaza, V. Lapoux, N. Keeley, N. Alamanos, E. C. Pollacco, F. Auger, A. Drouart, A. Gillibert, D. Beaumel, E. Becheva, Y. Blumenfeld, F. Delaunay, L. Giot, K. W. Kemper, L. Nalpas, A. Obertelli, A. Pakou, R. Raabe, P. Roussel-Chomaz, J.-L. Sida, J.-A. Scarpaci, S. Stepantsov, and R. Wolski, Phys. Rev. C **73**, 044301 (2006).
[69] I. Angeli and K. Marinova, At. Data Nucl. Data Tables **99**, 69 (2013).
[70] T. Otsuka, R. Fujimoto, Y. Utsuno, B. A. Brown, M. Honma, and T. Mizusaki, Phys. Rev. Lett. **87**, 082502 (2001).
[71] D. Tran, H. Ong *et al.*, Nat. Commun. **9**, 1594 (2018).